ACS APPLIED MATERIALS & INTERFACES

Research Article

www.acsami.org

General Self-Assembly Route toward Sparsely Studded Noble-Metal Nanocrystals inside Graphene Hollow Sphere Network for Ultrastable Electrocatalyst Utilization

Xinyuan Lou, Ping Wu,* Anping Zhang, Ruoqing Zhang, and Yawen Tang

Jiangsu Key Laboratory of New Power Batteries, Jiangsu Collaborative Innovation Center of Biomedical Functional Materials, School of Chemistry and Materials Science, Nanjing Normal University, Nanjing 210023, P. R. China

Supporting Information

ABSTRACT: Herein, we rationally design and construct a novel type of sparsely studded noble-metal nanocrystals inside graphene hollow sphere network (abbreviated as noble-metal@G HSN) through an electrostatic-attraction-directed self-assembly approach. The formation of Pt@G and Pd@G hollow sphere networks have been illustrated as examples using SiO_2 spheres as templates. Moreover, the electrocatalytic performance of the Pt@G HSN for methanol oxidation reaction has been examined as a proof-of-concept demonstration of the compositional and structural superiorities of noble-metal@G HSN toward electrocatalyst utilization. The as-prepared Pt@G HSN manifests higher catalytic activity and markedly enhanced long-term durability in comparison with commercial Pt/C catalyst.

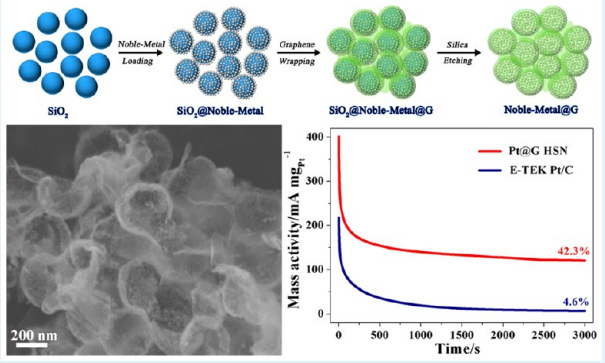

KEYWORDS: *noble-metal nanocrystals, graphene, hollow sphere network, electrocatalyst utilization, self-assembly route*

1. INTRODUCTION

Noble-metal nanocrystals possess exceptional physicochemical properties and have been intensively pursued for a wide variety of electrocatalyst utilization.[1−4] Generally, carbon supports including amorphous carbon, carbon nanotubes (CNTs), and graphene are required to immobilize noble-metal nanocrystals and improve structural stability and charge-transport capability of the hybrid catalysts.[5−8] Among these carbon matrices, graphene is of particular interest because of its high electrical conductivity and excellent mechanical flexibility, and thus could serve as an ideal conducting and supporting matrix for noble-metal electrocatalysts.[9−11] For example, a series of graphene-supported Pt and Pd hybrid catalysts are able to manifest enhanced electrocatalytic performance toward fuel (including methanol[12−18] and formic acid[19−21]) oxidation and oxygen reduction[22,23] reactions. However, in these hybrid catalysts, Pt and Pd nanocrystals are generally attached to the outer surfaces of the graphene matrices including wavy graphene,[12] vertically oriented graphene,[13,14] monolithic graphene,[15,16] graphene ribbon,[19] graphene quantum-dot,[22] and so forth. The noble-metal nanocrystals are directly exposed in outer environment and easily detached from carbon matrices and/or aggregated into large congeries, which leads to unsatisfied catalytic durability and greatly hinders their commercial application.

Recently, much research effort has been devoted to improve the long-term durability of noble-metal nanocrystals via pore-confinement structural design.[24−28] The confinement of noble-metal nanocrystals within pores of carbon supports can effectively suppress particle detachment/agglomeration and catalyst degradation. For example, the pore-confined Pt@C[27] and Pd@C[28] catalysts demonstrate markedly enhanced long-term electrocatalytic durability in comparison with partially confined and surface-located ones. However, the current research interest has been focused mainly on the Pt nanocrystals confined within amorphous and graphitic porous carbon supports.[24−28] The controllable synthesis of noble-metal nanocrystals inside graphene matrix remains a significant challenge, and it is very urgent to construct such pore-confined noble-metal@graphene nanohybrids for further-improved catalytic stability and practical utilization.

As inspired by this, we herein rationally design and construct a novel type of sparsely studded noble-metal nanocrystals inside graphene hollow sphere network (abbreviated as noble-metal@G HSN) through an electrostatic-attraction-directed self-assembly approach, as illustrated in Figure 1. SiO_2 spheres are chosen as templates in this synthetic route owing to its simple fabrication, low cost, and high productivity.[29] Subsequently, noble-metal nanocrystals and graphene layer are sparsely located and conformally wrapped on the SiO_2 templates in sequence based on electrostatic-attraction mechanism, resulting in SiO_2@noble-metal@G sphere network. After the etching of SiO_2 cores, noble-metal nanocrystals

Received: June 10, 2015
Accepted: August 25, 2015
Published: August 25, 2015

DOI: 10.1021/acsami.5b05116
ACS Appl. Mater. Interfaces 2015, 7, 20061−20067

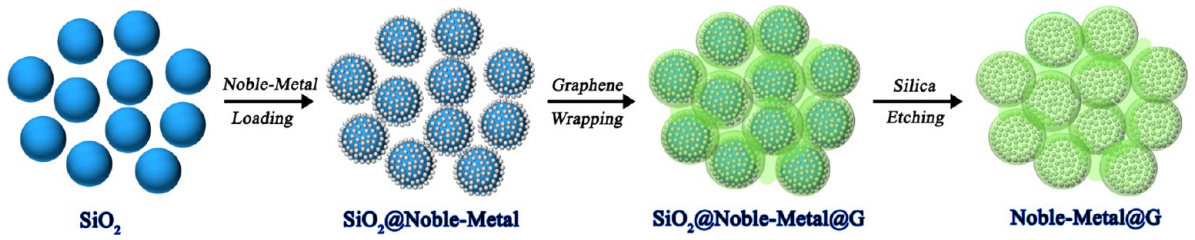

Figure 1. Schematic illustration for the formation of the noble-metal@G HSN.

are sparsely studded to the graphene hollow sphere network, yielding the final noble-metal@G HSN.

2. EXPERIMENTAL SECTION

Synthesis of the Pt@G and Pd@G Hollow Sphere Networks. First, uniform SiO_2 spheres with diameters of about 300 nm were obtained via a modified Stöber method. Second, SiO_2@Pt spheres were synthesized through an electrostatic-attraction-directed self-assembly approach. Typically, SiO_2 spherical templates were modified with poly(diallyldimethylammonium chloride) (PDDA) and poly(sodium 4-styrenesulfonate) (PSS) in sequence, resulting in positively charged PDDA/PSS/PDDA modified SiO_2 spheres.[29] Subsequently, 50 mg of polyelectrolyte-modified SiO_2 templates were dispersed in 50 mL of distilled water, and then 0.5 mmol $NaBH_4$ was added. After sonication for 10 min, a 20 mL aqueous solution containing 0.05 mmol H_2PtCl_6 and 0.15 mmol trisodium citrate were added dropwise and the mixture was further sonicated for 1 h. The resulting product was washed with distilled water and ethanol, yielding the SiO_2@Pt spheres. Third, the SiO_2@Pt spheres and graphene oxide (GO) (5:1 w/w) were dispersed in distilled water, stirred for 6 h, and then the GO component was reduced by $NaBH_4$ (weight ratio of 10:1 for $NaBH_4$:GO). The resulting product was washed and dried, resulting in SiO_2@Pt@G sphere network. Finally, the Pt@G HSN was obtained by dissolving the SiO_2 cores with a 2 M NaOH aqueous solution. Additionally, the Pd@G HSN was synthesized by using K_2PdCl_4 as a noble-metal precursor rather than H_2PtCl_6 with all other conditions unchanged.

Characterization. The morphology, composition, and structure of the products were characterized by X-ray powder diffraction (XRD, Rigaku D/max-RC), scanning electron microscopy (SEM, JEOL JSM-7600F), and high-resolution transmission electron microscopy (HRTEM, JEOL JEM-2010F, 200 kV) coupled with an energy-dispersive X-ray spectrometer (EDS, Thermo Fisher Scientific).

Electrochemical Measurement. The electrochemical experiments were tested with a CHI660C electrochemical analyzer and a conventional three electrode electrochemical cell. A Pt plate was applied as the auxiliary electrode, and a saturated calomel electrode (SCE) was utilized as the reference electrode. The working electrode was obtained as follows: an evenly distributed suspension of catalyst was prepared by sonicating the mixture of 2 mg of catalyst, i.e., Pt@G HSN, and 1 mL of ethanol for 30 min, and 5 μL of the resulting suspension was loaded on the surface of a glassy carbon electrode (3 mm in diameter, 0.07 cm^2). After drying, 2 μL of Nafion solution (5 wt %) was covered on the modified electrode surface, yielding the working electrode. Cyclic voltammetry (CV) tests were performed in N_2-purged 0.5 M H_2SO_4 solution with or without 0.5 M CH_3OH at a scan rate of 50 mV s^{-1}, whereas chronoamperometry curves were obtained in N_2-purged 0.5 M CH_3OH + 0.5 M H_2SO_4 solution for 3000 s at 0.6 V (vs. SCE). For comparison, the electrocatalytic performance of commercial 20 wt % Pt/C catalyst purchased from E-TEK Division (E-TEK Pt/C) was also investigated under the same conditions.

3. RESULTS AND DISCUSSION

As a typical example, the formation of Pt@G HSN was selected to illustrate the basic idea underlying this electrostatic-attraction-directed synthetic route. Figure 2 reveals the XRD

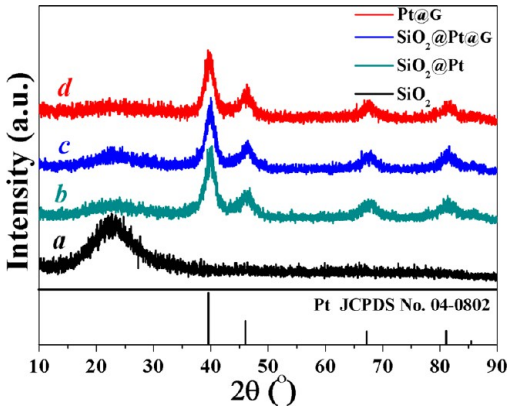

Figure 2. XRD patterns of the (curve a) SiO_2 spheres, (curve b) SiO_2@Pt spheres, (curve c) SiO_2@Pt@G sphere network, and (curve d) Pt@G HSN.

patterns of these samples in different stages of evolution. As can be seen, the crystalline phase can be well-matched to cubic Pt (curves *b*-*d*, JCPDS no. 04−0802) in SiO_2@Pt spheres, SiO_2@Pt@G sphere network, and Pt@G HSN, and the mean crystalline size of the Pt component can be calculated to be about 5 nm based on Scherrer equation. The morphological and structural features of the SiO_2@Pt and SiO_2@Pt@G intermediates were further examined by SEM and TEM (Figure 3). Figure 3a, b displays the SEM and TEM images of the SiO_2@Pt spheres. As observed, Pt nanocrystals are sparsely deposited on the surface of SiO_2 spheres, and no isolated nanocrystal can be observed in the sample except for the template surface. This phenomenon might be explained as follows. Because of the strong electrostatic-attraction between negatively charged reductant (BH_4^- ions) and positively charged polyelectrolyte-modified SiO_2, the subsequent reduction of $PtCl_6^{2-}$ to metallic Pt occurs only at the surface of SiO_2 templates, ensuring the entire deposition of Pt nanocrystals on SiO_2 spheres.[30] Additionally, the sparsely deposited rather than densely coated state of the SiO_2@Pt leaves exposed positively charged surface of polyelectolyte-modified SiO_2 templates. Thus, such sparsely located SiO_2@Pt spheres can be conformally wrapped by GO owing to the strong electrostatic-interaction between oppositely charged SiO_2@Pt and GO components together with the flexibility of GO matrix.[29] The GO shell could be converted into graphene matrix after subsequent chemical reduction process, yielding the SiO_2@Pt@G sphere network (Figure 3c, d). The observed folds and wrinkles over the entire spherical surface are characteristic of graphene shell, indicating the conformal wrapping and bridging of SiO_2@Pt spheres by graphene matrix. Additionally, a single SiO_2 spherical template is not fully wrapped by one piece of graphene, and might be simultaneously wrapped by multiple pieces of graphene.[31] The interspaces between the wrapped

DOI: 10.1021/acsami.5b05116
ACS Appl. Mater. Interfaces 2015, 7, 20061−20067

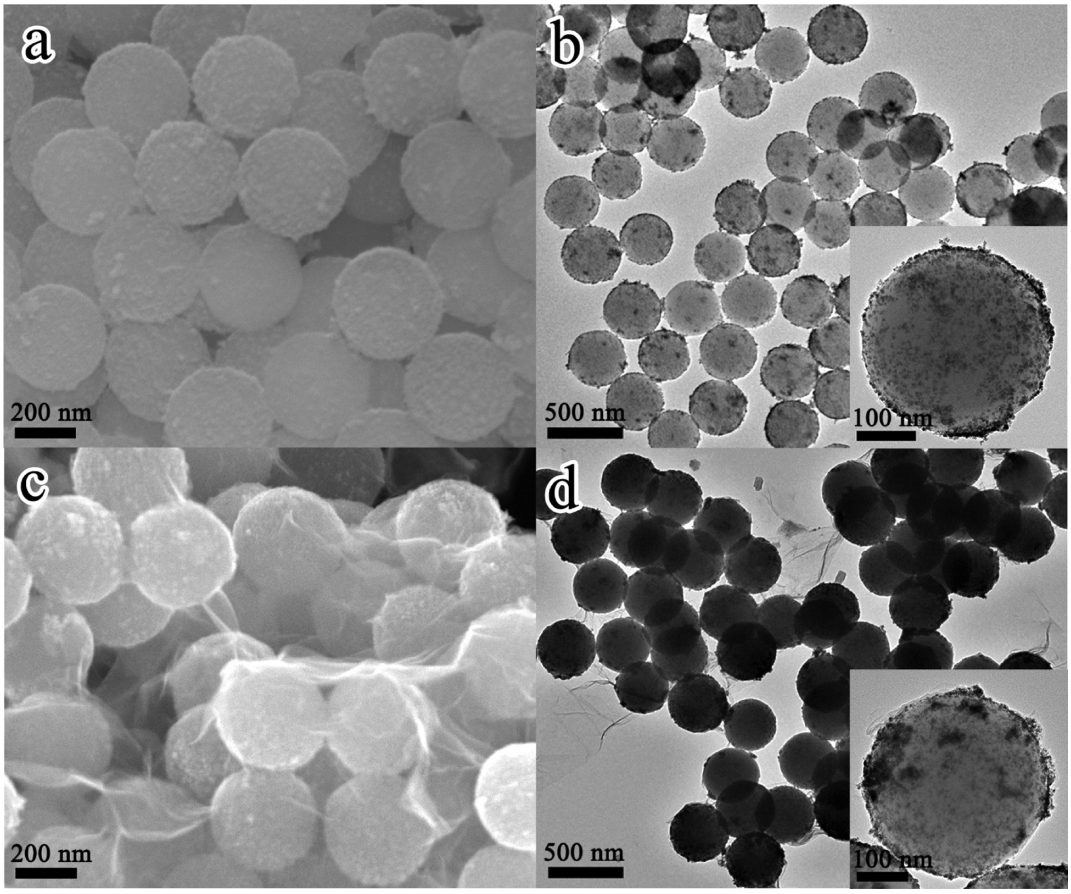

Figure 3. SEM and TEM images of the (a, b) SiO_2@Pt spheres and (c, d) SiO_2@Pt@G sphere network.

multiple pieces of graphene allow the access of aqueous solutions to the core regions of the sphere networks. Thus, the SiO_2 cores in SiO_2@Pt@G sphere network can be etched completely with NaOH aqueous solution, resulting in Pt@G HSN. Moreover, the aqueous electrolytes can easily penetrate into the internal part of graphene hollow sphere and contact with Pt nanocrystals during the electrocatalytic utilization of the Pt@G HSN catalyst.

Figure 4a–d reveals the SEM and TEM images of the Pt@G HSN with different magnifications. As observed, the graphene matrix exists in the form of three-dimensioanl (3D) interconnected hollow sphere network since the SiO_2@Pt spheres are conformally wrapped and bridged by graphene shell in the SiO_2@Pt@G intermediate. The self-assembled 3D interconnected network holds the structural superiorities of both nanosized building units and microsized assemblies, and is able to manifest improved structural stability, charge-transport capability, and thus enhanced electrochemical performances inlcuding lithium-storage and electrocatalytic utilization.[16,21,29,32] The selected-area electron diffraction (SAED) pattern shows typical diffraction rings characteristic of (111), (200), (220), and (311) planes of cubic Pt (Figure 4c, inset), indicating the poly crystalline nature of Pt component within the hybrid network. More specifically, numerous Pt nanocrystals are well-confined within the graphene hollow sphere building units, and sparsely studded to the inside surface of graphene matrix. The unique sparsely studded strcutrue can significantly suppress the detachment and agglomeration of noble-metal nanoparticles, and are anticipated to manifest enhanced electrocatalytic durability.[24−28] Figure 4e displays the HRTEM image of the Pt@G HSN. The observed three kinds of lattice fringes with spacings of 0.226, 0.196, and 0.139 nm correspond to the (111), (200), and (220) planes of cubic Pt nanocrystals, respectively. Figure 4f reveals the TEM-EDS elemental mappings of C (yellow) and Pt (green) and EDS spectrum of the Pt@G HSN. The observed platinum elemental signal is consistent with carbon signal and is uniformly distributed over the chosen area, further confirming the homogeneous confinement of Pt nanocrystals within graphene matrix. Additinally, the Pt content in the Pt@G HSN can be determined to be about 36.8% by weight from EDS spectrum.

To verify the versatility of this methodology, we have applied the synthetic route for the formation of Pd@G HSN. Figure 5 displays the morphological, compositional, and structural features of the Pd@G HSN. The TEM image clearly reveals the 3D interconnected hollow sphere struture of graphene matrix (Figure 5a). Moreover, the magnified TEM image (Figure 5b) and its SAED pattern (Figure 5a, inset) of a single hollow sphere indicate that numerous Pd nanocrystals are confined within the hollow sphere and sparsely attached to the inside surface of graphene shell. Additioanlly, the HRTEM image (Figure 5c) and TEM-EDS elemental mappings (Figure 5d) further confirm the formation of Pd component and the efficient encapsulation and uniform distribution of Pd nanocrystals in graphene matrix.

As a proof-of-concept demonstration of the compositional and structural superiorities of noble-metal@G HSN toward electrocatalyst utilization, the electrocatalytic performance of the Pt@G HSN for methanol oxidation reaction has been examined in comparison with commercial E-TEK Pt/C catalyst.

DOI: 10.1021/acsami.5b05116
ACS Appl. Mater. Interfaces 2015, 7, 20061−20067

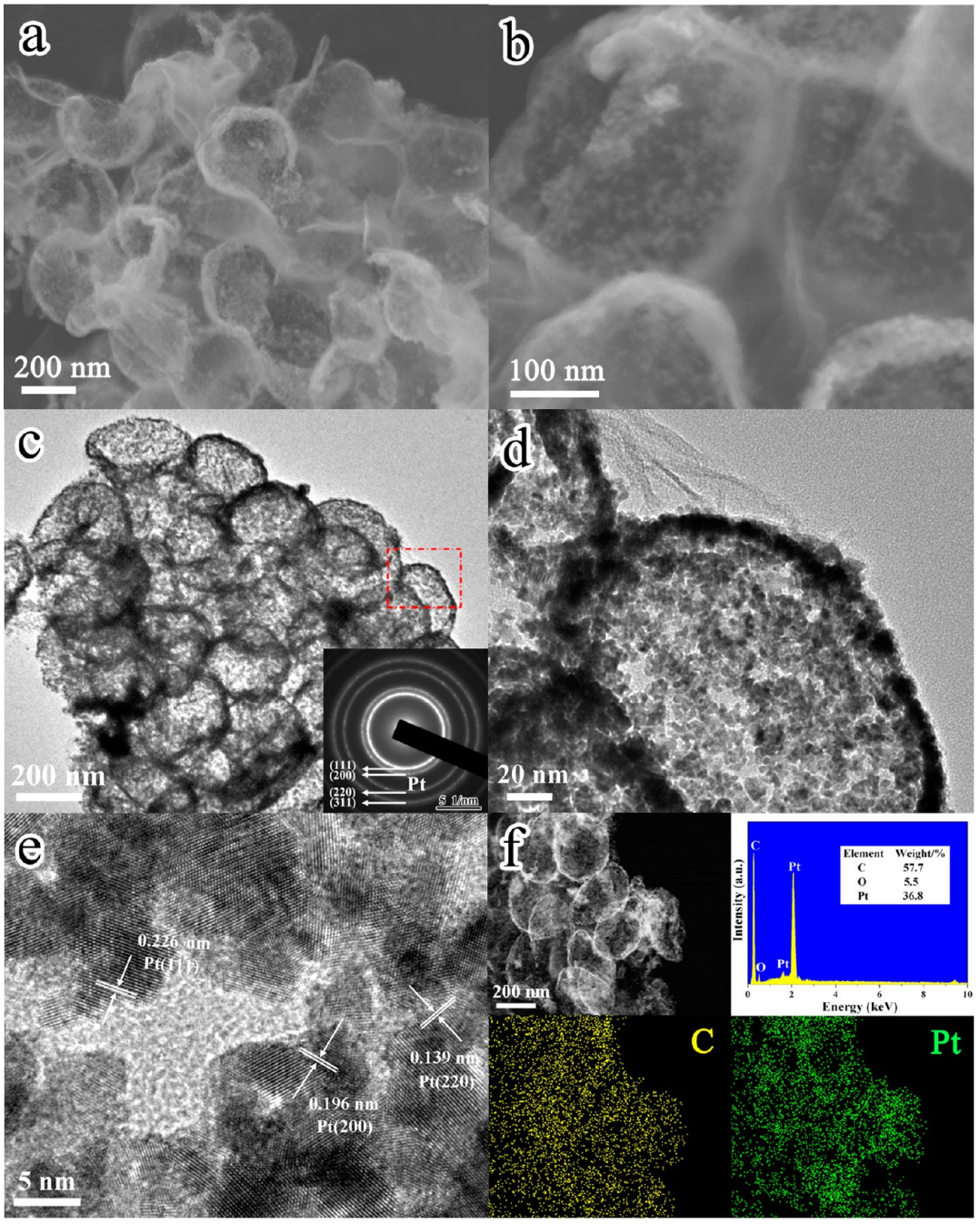

Figure 4. Morphological, compositional, and structural features of the Pt@G HSN: (a, b) SEM images, (c, d) TEM images and the corresponding SAED pattern, (e) HRTEM image, and (f) TEM-EDS elemental mappings and EDS spectrum.

Figure 6 shows the CV curves of the Pt@G HSN and E-TEK Pt/C catalysts in 0.5 M H_2SO_4 solution at a scan rate of 50 mV s^{-1}. As observed, both catalysts exhibit typical features of hydrogen adsorption/desorption within the potential range of −0.24−0.1 V, and the integrated charge of these peaks reflects the number of Pt active sites. Herein, the electrochemically active surface area (ECSA) of Pt-based catalysts is calculated by integrating the area of hydrogen desorption wave,[12] and the values for the Pt@G HSN and E-TEK Pt/C catalysts are determined to be 31.2 and 18.8 m^2 g^{-1}, respectively. The lager ECSA value of the Pt@G HSN can be attributed to the higher dispersion of Pt nanocrystals on graphene matrix and improved charge-transport capability of the 3D interconnected network and thus the enhanced mass utilization of Pt component, which is also favorable for the enhancement of electrocatalytic activity.[9,10]

Figure 7a depicts the CV curves of the Pt@G HSN and E-TEK Pt/C catalysts in 0.5 M CH_3OH + 0.5 M H_2SO_4 solution at a scan rate of 50 mV s^{-1}. As can be seen, the Pt@G HSN manifests higher electrocatalytic activity than E-TEK Pt/C catalyst. For example, the ECSA-normalized oxidation peak current of the Pt@G HSN is slightly higher than that of E-TEK Pt/C catalyst (Figure S1), and more apparently, the mass normalized value for the Pt@G HSN (360.4 mA mg_{Pt}^{-1}) is 1.8 times that for the E-TEK Pt/C catalyst (201.3 mA mg_{Pt}^{-1}). The reason can be explained as follows. The sparsely studded noble-

DOI: 10.1021/acsami.5b05116
ACS Appl. Mater. Interfaces 2015, 7, 20061−20067

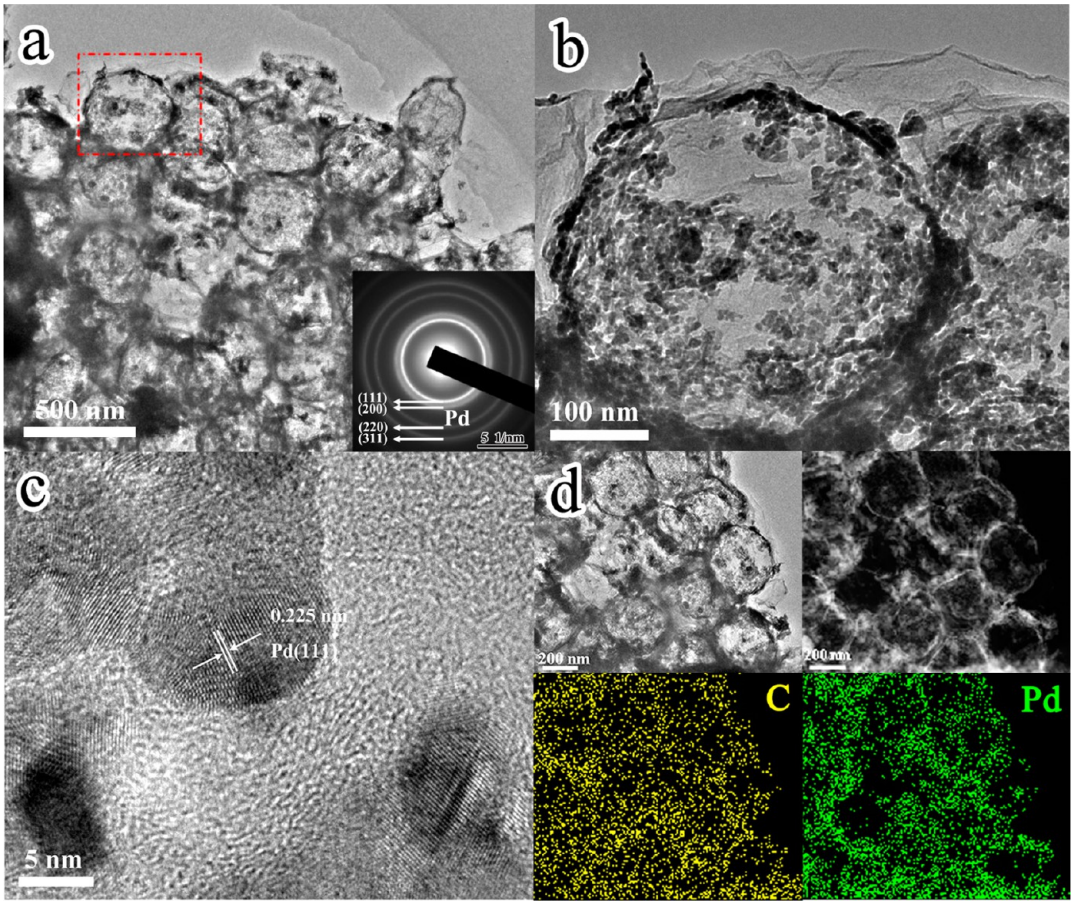

Figure 5. Morphological, compositional, and structural features of the Pd@G HSN: (a, b) TEM images and the corresponding SAED pattern, (c) HRTEM image, and (d) TEM-EDS elemental mappings.

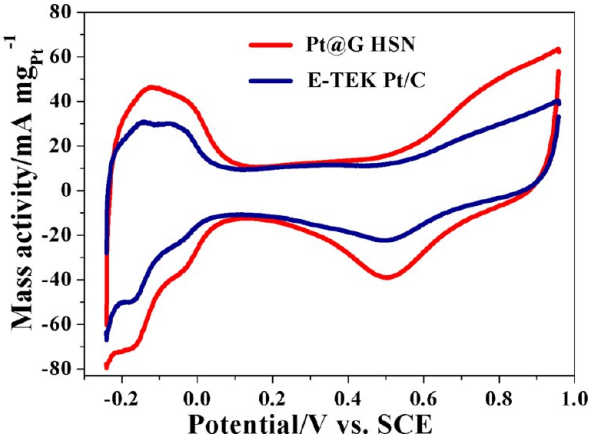

Figure 6. CV curves of the Pt@G HSN and E-TEK Pt/C catalysts in N_2-purged 0.5 M H_2SO_4 solution at a scan rate of 50 mV s^{-1}.

metal@G structure leads to a high dispersion of Pt nanocrystals within graphene hollow sphere, and the 3D interconnected structure of graphene network is beneficial for improved charge-transport capability of the noble-metal@G catalysts. Thus, the Pt@G HSN is able to exhibit enhanced mass utilization and reaction kinetics and higher electrocatalytic activity toward methanol oxidation reaction.

More importantly, the unique structural and compostional features of the noble-metal@G HSN are favorable for their long-term catalytic stability, which can be confirmed by chronoamperometric tests. Figure 7b displays the chronoamperometry curves of the Pt@G HSN and E-TEK Pt/C catalysts in 0.5 M CH_3OH + 0.5 M H_2SO_4 solution at 0.6 V (vs. SCE). After 3000 s, the methanol oxidation currents of the Pt@G HSN and E-TEK Pt/C catalysts decrease to 42.3 and 4.6% of their initial values (take the data of 10 s), respectively, demonstrating significantly enhanced catalytic durability of the Pt@G HSN toward methanol electro-oxidation. Similarly, the enhanced electrocatalytic stability toward formic acid oxidation has been observed from the Pd@G HSN compared with conventional Vulcan XC-72-Pd (Pd/XC-72) catalyst (Figure S2). After 3000 s, the formic acid oxidation currents of the Pd@G HSN and Pd/XC-72 catalysts decrease to 20.8% and 2.2% of their initial values (take the current of 10 s), respectively (Figure S2b). The sparsely studded structural and compostional design of the noble-metal@G HSN can significantly suppress the detachment and agglomeration of noble-metal nanocrystals, which can be responsible for their excellent long-term electrocatalytic durability.[24−28]

4. CONCLUSION

We propose a general electrostatic-attraction-directed self-assembly route for the construction of sparsely studded noble-metal nanocrystals inside graphene hollow sphere network (noble-metal@G HSN). The formation of Pt@G and Pd@G hollow sphere networks have been illustrated as examples using SiO_2 spheres as templates. Moreover, the electrocatalytic performance of the Pt@G HSN for methanol electro-oxidation

DOI: 10.1021/acsami.5b05116
ACS Appl. Mater. Interfaces 2015, 7, 20061−20067

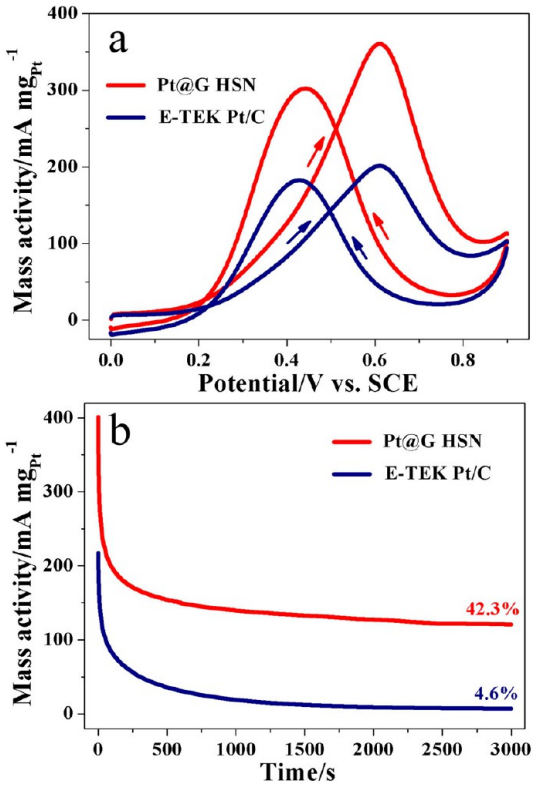

Figure 7. (a) CV curves of the Pt@G HSN and E-TEK Pt/C catalysts in N_2-purged 0.5 M CH_3OH + 0.5 M H_2SO_4 solution at a scan rate of 50 mV s^{-1}, (b) chronoamperometry curves of the Pt@G HSN and E-TEK Pt/C catalysts in N_2-purged 0.5 M CH_3OH + 0.5 M H_2SO_4 solution at 0.6 V (vs. SCE).

has been examined as a proof-of-concept demonstration of their compositional and structural superiorities toward electrocatalyst utilization. Compared with commercial Pt/C catalyst, the Pt@G HSN manifests significantly enhanced electrocatalytic performance in terms of higher activity and enhanced long-term durability, making it an ideal anodic catalyst candidate for practical utilization. Moreover, the proposed sparsely studded structural and compostional design of the noble-metal@G HSN would shed some light on the construction of supported electrocatalysts with superb long-term durability.

■ ASSOCIATED CONTENT

Supporting Information

The Supporting Information is available free of charge on the ACS Publications website at DOI: 10.1021/acsami.5b05116.

ECSA-normalized CV curves of the Pt@G HSN; electrocatalytic performance of the Pd@G HSN toward formic acid oxidation reaction (PDF)

■ AUTHOR INFORMATION

Corresponding Author

*E-mail: zjuwuping@njnu.edu.cn.

Notes

The authors declare no competing financial interest.

■ ACKNOWLEDGMENTS

We appreciate the financial supports from the National Natural Science Foundation of China (21376122, 21273116, and 51401110), Natural Science Foundation of Jiangsu Province (BK20130900), and a project funded by the Priority Academic Program Development of Jiangsu Higher Education Institutions.

■ DEDICATION

This paper is dedicated to the memory of Professor Tianhong Lu (1943−2014).

■ REFERENCES

(1) Guo, S.; Wang, E. Noble Metal Nanomaterials: Controllable Synthesis and Application in Fuel Cells and Analytical Sensors. *Nano Today* **2011**, *6*, 240−264.

(2) Zhang, H.; Jin, M.; Xia, Y. Noble-Metal Nanocrystals with Concave Surfaces: Synthesis and Applications. *Angew. Chem., Int. Ed.* **2012**, *51*, 7656−7673.

(3) Manokaran, J.; Muruganantham, R.; Muthukrishnaraj, A.; Balasubramanian, N. Platinum-Polydopamine@SiO_2 Nanocomposite Modified Electrode for the Electrochemical Determination of Quercetin. *Electrochim. Acta* **2015**, *168*, 16−24.

(4) Li, H.; Wang, J.; Liu, S.; Wang, H.; Su, P.; Wu, J.; Li, J. A Nanoporous Oxide Interlayer Makes a Better Pt Catalyst on a Metallic Substrate: Nanoflowers on a Nanotube Bed. *Nano Res.* **2014**, *7*, 1007−1017.

(5) Su, D. S.; Perathoner, S.; Centi, G. Nanocarbons for the Development of Advanced Catalysts. *Chem. Rev.* **2013**, *113*, 5782−5816.

(6) Huang, H.; Wang, X. Recent Progress on Carbon-Based Support Materials for Electrocatalysts of Direct Methanol Fuel Cells. *J. Mater. Chem. A* **2014**, *2*, 6266−6291.

(7) Wang, Q.; Geng, B.; Tao, B. A Facile Room Temperature Chemical Route to Pt Nanocube/Carbon Nanotube Heterostructures with Enhanced Electrocatalysis. *J. Power Sources* **2011**, *196*, 191−195.

(8) Zhang, J. J.; Wang, Z. B.; Li, C.; Zhao, L.; Liu, J.; Zhang, L. M.; Gu, D. M. Multiwall-Carbon Nanotube Modified by N-Doped Carbon Quantum Dots as Pt Catalyst Support for Methanol Electrooxidation. *J. Power Sources* **2015**, *289*, 63−70.

(9) Xia, B. Y.; Yan, Y.; Wang, X.; Lou, X. W. Recent Progress on Graphene-Based Hybrid Electrocatalysts. *Mater. Horiz.* **2014**, *1*, 379−399.

(10) Liu, M.; Zhang, R.; Chen, W. Graphene-Supported Nanoelectrocatalysts for Fuel Cells: Synthesis, Properties, and Applications. *Chem. Rev.* **2014**, *114*, 5117−5160.

(11) Huang, X.; Yin, Z.; Wu, S.; Qi, X.; He, Q.; Zhang, Q.; Yan, Q.; Boey, F.; Zhang, H. Graphene-Based Materials: Synthesis, Characterization, Properties, and Applications. *Small* **2011**, *14*, 1876−1902.

(12) Shao, J. J.; Li, Z. J.; Zhang, C.; Zhang, L. F.; Yang, Q. H. A Wavy Graphene/Platinum Hybrid with Increased Electroactivity for the Methanol Oxidation Reaction. *J. Mater. Chem. A* **2014**, *2*, 1940−1946.

(13) Yang, L.; Tang, Y.; Luo, S.; Liu, C. B.; Song, H.; Yan, D. Palladium Nanoparticles Supported on Vertically Oriented Reduced Graphene Oxide for Methanol Electro-Oxidation. *ChemSusChem* **2014**, *7*, 2907−2913.

(14) Zhang, X.; Wu, E.; Hu, D.; Bo, Z.; Zhu, W.; Yu, K.; Yu, C.; Wang, Z.; Yan, J.; Cen, K. Highly-Branched Vertically-Oriented Graphene Nanosheets with Dense Open Graphitic Edge Planes as Pt Support for Methanol Oxidation. *Phys. Status Solidi B* **2014**, *251*, 829−837.

(15) Qiu, H.; Dong, X.; Sana, B.; Peng, T.; Paramelle, D.; Chen, P.; Lim, S. Ferritin-Templated Synthesis and Self-Assembly of Pt Nanoparticles on a Monolithic Porous Graphene Network for Electrocatalysis in Fuel Cells. *ACS Appl. Mater. Interfaces* **2013**, *5*, 782−787.

(16) Maiyalagan, T.; Dong, X.; Chen, P.; Wang, X. Electrodeposited Pt on Three-Dimensional Interconnected Graphene as a Free-Standing Electrode for Fuel Cell Application. *J. Mater. Chem.* **2012**, *22*, 5286−5290.

(17) Li, L.; Zhang, J.; Liu, Y.; Zhang, W.; Yang, H.; Chen, J.; Xu, Q. Facile Fabrication of Pt Nanoparticles on 1-Pyrenamine Function-

DOI: 10.1021/acsami.5b05116
ACS Appl. Mater. Interfaces 2015, 7, 20061−20067

alized Graphene Nanosheets for Methanol Electrooxidation. *ACS Sustainable Chem. Eng.* **2013**, *1*, 527−533.
(18) Sahu, S. C.; Samantara, A. K.; Dash, A.; Juluri, R. R.; Sahu, R. K.; Mishra, B. K.; Jena, B. K. Graphene-Induced Pd Nanodendrites: A High Performance Hybrid Nanoelectrocatalyst. *Nano Res.* **2013**, *6*, 635−643.
(19) Wang, S.; Manthiram, A. Graphene Ribbon-Supported Pd Nanoparticles as Highly Durable, Efficient Electrocatalysts for Formic Acid Oxidation. *Electrochim. Acta* **2013**, *88*, 565−570.
(20) Yang, S.; Dong, J.; Yao, Z.; Shen, C.; Shi, X.; Tian, Y.; Lin, S.; Zhang, X. One-Pot Synthesis of Graphene-Supported Monodisperse Pd Nanoparticles as Catalyst for Formic Acid Electro-Oxidation. *Sci. Rep.* **2014**, *4*, 4501.
(21) Wang, Y.; Liu, H.; Wang, L.; Wang, H.; Du, X.; Wang, F.; Qi, T.; Lee, J. M.; Wang, X. Pd Catalyst Supported on a Chitosan-Functionalized Large-Area 3D Reduced Graphene Oxide for Formic Acid Electrooxidation Reaction. *J. Mater. Chem. A* **2013**, *1*, 6839−6848.
(22) Song, Y.; Chen, S. Graphene Quantum-Dot-Supported Platinum Nanoparticles: Defect-Mediated Electrocatalytic Activity in Oxygen Reduction. *ACS Appl. Mater. Interfaces* **2014**, *6*, 14050−14060.
(23) Zhu, J.; Xiao, M.; Zhao, X.; Liu, C.; Ge, J.; Xing, W. Strongly Coupled Pt Nanotubes/N-Doped Graphene as Highly Active and Durable Electrocatalysts for Oxygen Reduction Reaction. *Nano Energy* **2015**, *13*, 318−326.
(24) Wu, Z.; Lv, Y.; Xia, Y.; Webley, P. A.; Zhao, D. Ordered Mesoporous Platinum@Graphitic Carbon Embedded Nanophase as a Highly Active, Stable, and Methanol-Tolerant Oxygen Reduction Electrocatalyst. *J. Am. Chem. Soc.* **2012**, *134*, 2236−2245.
(25) Galeano, C.; Meier, J. C.; Peinecke, V.; Bongard, H.; Katsounaros, I.; Topalov, A. A.; Lu, A.; Mayrhofer, K. J. J.; Schüth, F. Toward Highly Stable Electrocatalysts *via* Nanoparticle Pore Confinement. *J. Am. Chem. Soc.* **2012**, *134*, 20457−20465.
(26) Zhang, C.; Xu, L.; Shan, N.; Sun, T.; Chen, J.; Yan, Y. Enhanced Electrocatalytic Activity and Durability of Pt Particles Supported on Ordered Mesoporous Carbon Spheres. *ACS Catal.* **2014**, *4*, 1926−1930.
(27) Yang, C.; Zhou, M.; Xu, Q. Confining Pt Nanoparticles in Porous Carbon Structures for Achieving Durable Electrochemical Performance. *Nanoscale* **2014**, *6*, 11863−11870.
(28) Datta, A.; Kapri, S.; Bhattacharyya, S. Enhanced Catalytic Activity of Palladium Nanoparticles Confined inside Porous Carbon in Methanol Electro-Oxidation. *Green Chem.* **2015**, *17*, 1572−1580.
(29) Wu, P.; Wang, H.; Tang, Y.; Zhou, Y.; Lu, T. Three-Dimensional Interconnected Network of Graphene-Wrapped Porous Silicon Spheres: In Situ Magnesiothermic-Reduction Synthesis and Enhanced Lithium-Storage Capabilities. *ACS Appl. Mater. Interfaces* **2014**, *6*, 3546−3552.
(30) Du, N.; Zhang, H.; Yang, D. One-Dimensional Hybrid Nanostructures: Synthesis *via* Layer-by-Layer Assembly and Applications. *Nanoscale* **2012**, *4*, 5517−5526.
(31) Chen, C. M.; Zhang, Q.; Huang, C. H.; Zhao, X. C.; Zhang, B. S.; Kong, Q. Q.; Wang, M. Z.; Yang, Y. G.; Caia, R.; Su, D. S. Macroporous 'Bubble' Graphene Film via Template-Directed Ordered-Assembly for High Rate Supercapacitors. *Chem. Commun.* **2012**, *48*, 7149−7151.
(32) Kim, H. K.; Park, S. H.; Yoon, S. B.; Lee, C. W.; Jeong, J. H.; Roh, K. C.; Kim, K. B. In Situ Synthesis of Three-Dimensional Self-Assembled Metal Oxide−Reduced Graphene Oxide Architecture. *Chem. Mater.* **2014**, *26*, 4838−4843.

DOI: 10.1021/acsami.5b05116
ACS Appl. Mater. Interfaces 2015, 7, 20061−20067